A&A 424, 1049–1053 (2004)
DOI: 10.1051/0004-6361:20041380

Astronomy & Astrophysics

Asymmetrical appearance of dark-cored filaments in sunspot penumbrae

P. Sütterlin[1], L. R. Bellot Rubio[2], and R. Schlichenmaier[2]

[1] Sterrekundig Instituut Utrecht, Postbus 80 000, 3508 TA Utrecht, The Netherlands
e-mail: P.Suetterlin@astro.uu.nl
[2] Kiepenheuer Institut für Sonnenphysik, Schöneckstr. 6, 79104 Freiburg, Germany

Received 1 June 2004 / Accepted 2 June 2004

Abstract. Recent sunspot observations at unprecedented resolution have led to the discovery of dark cores in the bright filaments that form the penumbra (Scharmer et al. 2002). The discovery paper considered spots at disk center only, so the properties of the dark-cored filaments remain largely unknown. Here we analyze a speckle-reconstructed time series of *G*-band and blue continuum images of a sunspot acquired with the Dutch Open Telescope. The target was located at an heliocentric angle of 27 deg. We confirm the existence of dark-cored penumbral filaments also in spots outside the disk center, and report on distinct differences between the center and limb-side penumbra. In the inner center-side penumbra, filaments are detected as two narrow bright streaks separated by a central obscuration. These structures move together as a single entity. On the limb side, dark cores are hardly seen. The time series is used to determine the sizes (~200−250 km), proper motions (~280 m s^{-1}), and lifetimes (≲45 min) of typical dark-cored filaments.

Key words. Sun: sunspots – Sun: magnetic fields – Sun: photosphere – magnetohydrodynamics

1. Introduction

The nature of sunspot penumbrae is still subject to intense debate, both observational and theoretical (see, e.g., the reviews by Solanki 2003; Bellot Rubio 2004; Schlichenmaier 2002). The penumbra consists of a pattern of radially aligned bright and dark filaments. The small size of these filaments makes it difficult to characterize their properties and structure. Recently, 0.1 arcsec observations with the Swedish 1-m Solar Telescope have revealed a hitherto unexpected feature of bright penumbral filaments: at this resolution they often show internal substructure in the form of two sharp, bright edges separated by a central dark core (Scharmer et al. 2002; Rouppe van der Voort et al. 2004). The edges of the filament and the dark cores move synchronously and follow the same trajectories, suggesting that they are intimately connected. This internal structuring may hold the key to understand the nature of penumbral filaments.

No explanation for the existence of dark cores has been offered yet, although first attempts to model them are underway (Ruiz Cobo, private communication). In order to facilitate theoretical efforts, it is necessary to characterize the properties and visibility of dark-cored penumbral filaments at different viewing angles. It is also important to confirm the very existence of such dark cores: so far, they have been observed in just two spots and with only one telescope.

In this paper we present *G*-band and blue continuum filtergrams of a sunspot located at an heliocentric angle of 27 deg. The observations were taken with the Dutch Open Telescope (DOT) during more than 3.5 h. Our data confirm the existence of the dark-cored penumbral filaments reported by Scharmer et al. (2002), and demonstrate that spots away from the center of the solar disk also show them. For the first time, we detect clear differences in the visibility of dark-cored filaments in the center and limb-side penumbra. Dark cores are very distinct on the center side, but not on the limb side.

Section 2 gives details of the observations and the speckle reconstruction. In Sect. 3 we present the best filtergrams and describe the appearance of the dark-cored filaments. A few typical examples are selected for estimating their sizes, proper motions, and lifetimes. Finally, Sect. 4 summarizes our findings and speculates on the origin of the center/limb asymmetry in the occurrence of dark cores.

2. Observations and data processing

On August 9, 2003 a four-wavelength image series of an isolated spot (NOAA 10425) was obtained with the DOT at the Observatorio del Roque de los Muchachos (La Palma, Spain) during UT 08:25−11:58. The observations were part of a coordinated campaign with the Vacuum Tower Telescope (Observatorio del Teide, Tenerife, Spain), where full vector polarimetry of the same target was performed at lower spatial resolution. The regular sunspot was observed at an heliocentric angle of 27 deg ($\mu = 0.89$).

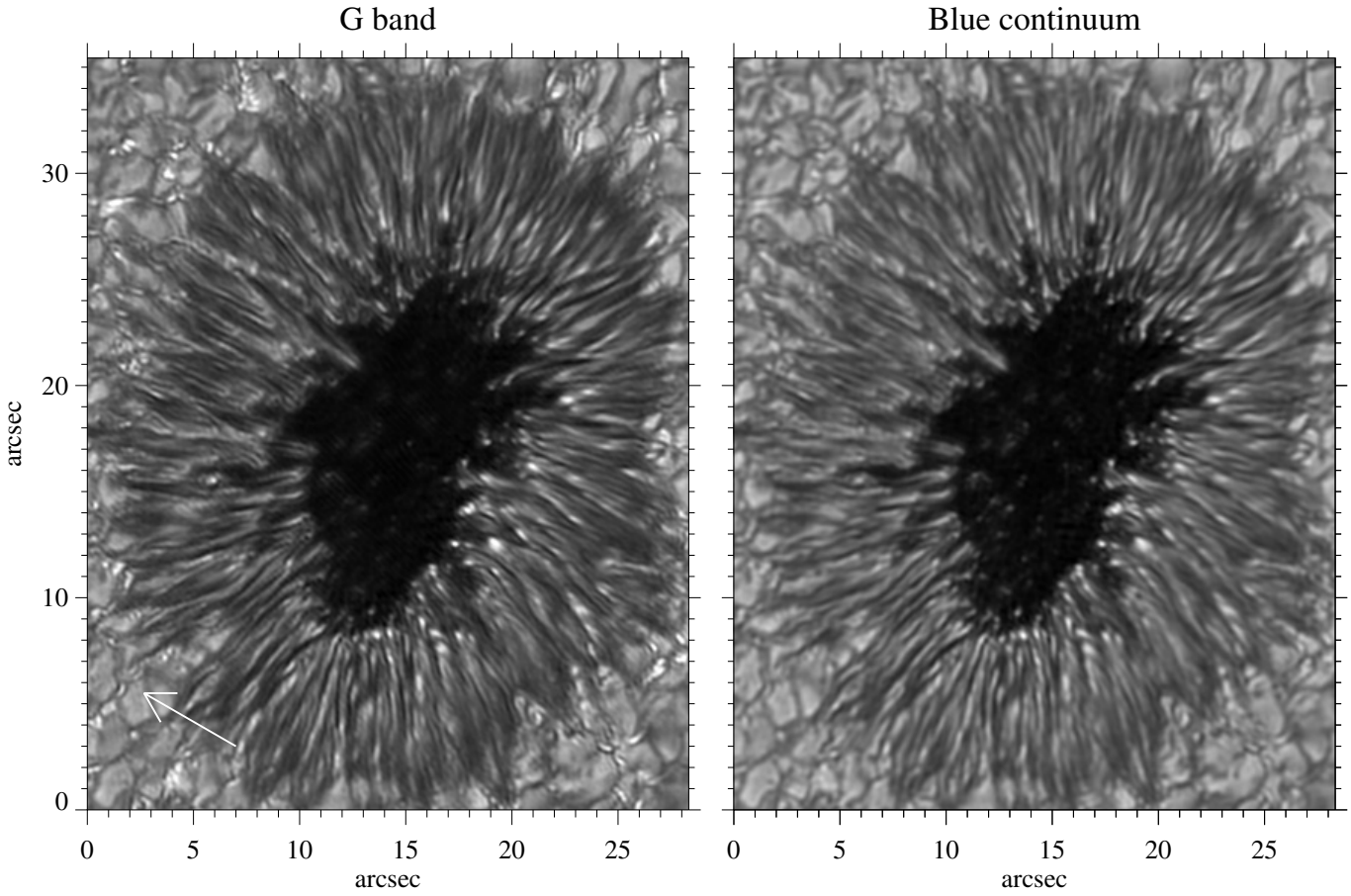

Fig. 1. Subfield of one of our best *G*-band (*left*) and blue continuum (*right*) filtergrams. The arrow marks the direction to disk center. The full field of view amounts to 87×70 arcsec^2. The images are corrected for atmospheric distortions using the speckle masking method, and reach the theoretical resolution limit of the telescope of 0.2 arcsec.

The series consists of simultaneous speckle bursts taken every 60 s in the *G* band (430.5 ± 0.5 nm), Ca II H (396.8 ± 0.06 nm), blue (432.0 ± 0.3 nm) and red (655.0 ± 0.3 nm) continuum. Each burst contains 100 individual frames, covering a field of view of 92×73 arcsec^2, with 0.071 arcsec per pixel. The exposure times were 1 ms for the broad-band images and 12 ms for Ca. The seeing quality, as measured by the Fried parameter r_0 at 430.5 nm, varied between 4.5 cm and 10.6 cm with an average of 7.0 cm, ranking it as a standard quality series (cf. Fig. 3 in Rutten et al. 2004). Speckle reconstruction (Weigelt 1977; de Boer & Kneer 1992; de Boer 1993) has been applied to improve the spatial resolution of the observations. For r_0 values larger than 7 cm, the speckle masking algorithm is able to deliver diffraction-limited (0.2 arcsec) images. So far only the first three wavelengths have been reconstructed. Further details on the optical setup of the DOT, the camera system, and the speckle reconstruction applied to the raw data are given in Rutten et al. (2004).

The reconstructed images have been used to create movies[1] in the following way. To compensate for the imperfect reconstruction in case of bad seeing ($r_0 < 7$ cm), the Fourier amplitudes of the respective images were enhanced so that the radially averaged power spectrum matched that of the fully reconstructed images. All images of one wavelength were then temporally aligned using Fourier correlation techniques. The image segmentation into isoplanar subfields during the speckle reconstruction leaves some residual image distortion that is only seen when playing the frames as a movie. Those distortions were removed using local correlation tracking and polynomial warping ("rubbersheeting"). Next, the data cubes for all wavelengths were clipped to the common field of view (87×70 arcsec^2). Finally, the data cubes were low-pass filtered using a cone-shaped filter in the three-dimensional (k_x, k_y, ν) Fourier space where the opening angle of the cone corresponds to 7 km s^{-1}. This removed all apparently supersonic intensity signals stemming from oscillatory phenomena.

3. Results

3.1. Individual filtergrams

In Fig. 1 we display a subfield of one of the best *G*-band and blue continuum images of NOAA 10425 taken at 10:55 UT (the Fried parameter was $r_0 = 9.3$ cm). The arrow points toward disk center. The penumbra exhibits clear differences between the center and the limb side: the almost point-like bright penumbral grains at the border between umbra and penumbra are most prominent on the limb side. Similar structures on the center side, while also visible, have much lower intensity contrasts, as already pointed out by Tritschler et al. (2004).

[1] Available at the DOT data base:
`http://hst33127.phys.uu.nl/DOT/Data/2003_08_09/`

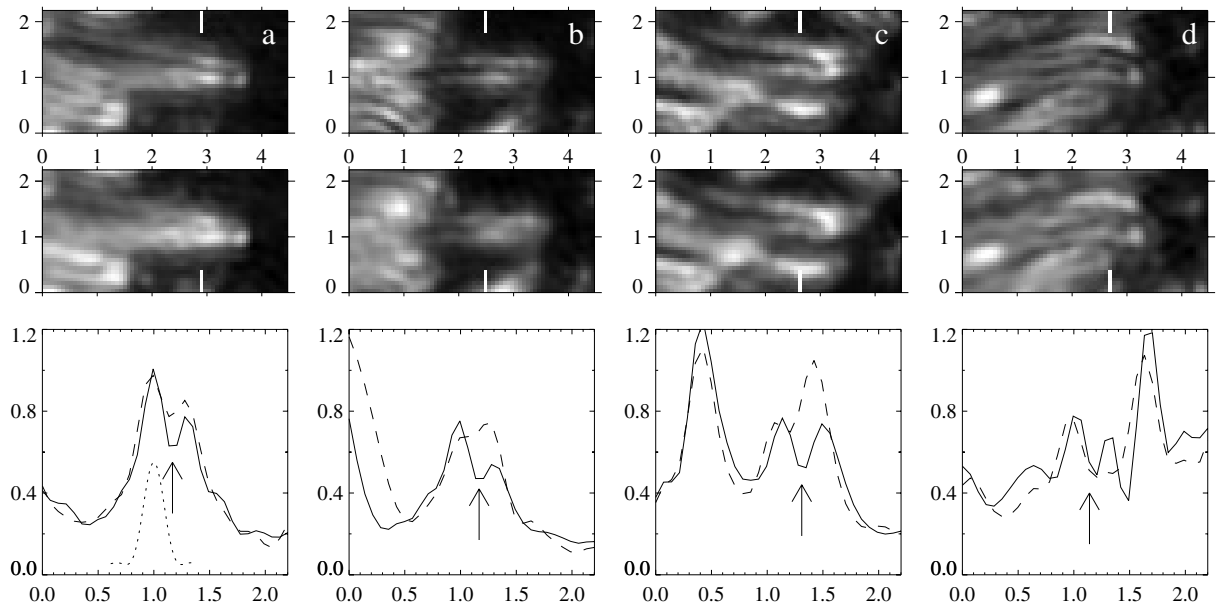

Fig. 2. Examples of dark-cored filaments observed in the center-side penumbra. Each of the columns shows (*from top to bottom*) *G*-band intensity, continuum intensity, and a bottom-to-top cut through the structure at the position indicated in the images. Distances are expressed in arcsec. The intensities are normalized to the mean quiet sun intensity. Each image is rotated to similar orientation. *Solid*: *G* band. *Dashed*: blue continuum. The dotted profile in the first plot depicts the Airy point-spread function of the telescope at 430.5 nm, with a *FWHM* of 0.2 arcsec.

Figure 1 also shows bright filaments with dark cores in the center-side penumbra, especially near the umbra where they stand out over a less crowded background. By contrast, dark cores are hardly seen on the limb side. This is difficult to prove with just one image, the claim is based on careful inspection of the time-lapse movie and judging the evolution of structures (see `AR10425a.mpg` available as online material).

Figure 2 displays some examples of the dark-cored filaments we observe on the center side. For each example a–d, the *G*-band image (top), the blue continuum image (middle) and two intensity profiles (bottom) at the position indicated by a white tick mark in the images are shown. The appearance of these structures is very similar to that described by Scharmer et al. (2002): they consist of two lateral brightenings separated by a darker region in between. The brightenings and the central obscuration move synchronously following the same trajectories (see Sect. 3.2). The inner footpoint of the dark-cored filaments is usually associated with a penumbral grain or peripheral umbral dot, but these bright structures are only seldom centered on the dark cores: in most cases they are seen closer to one of the lateral brightenings. The two edges of the filaments may possess the same or different intensities, with a typical average value of 0.7 times the mean photospheric intensity. The intensity drop in the dark core is 0.1–0.2 in units of the mean photospheric intensity. For the bright filaments there is no systematic intensity difference between *G* band and blue continuum, however the dark cores exhibit larger intensity dips in the *G* band. This is in line with the rms intensity variations in the two wavelength bands: the *G*-band contrast is largely enhanced in the penumbra. We do not find evidence for dark cores in our Ca images.

A comparison of the intensity profiles of the dark-cored filaments with the theoretical point-spread function of the DOT (first plot in Fig. 2) shows that the lateral brightenings are unresolved. Giving widths of structures under these conditions is not meaningful, so we restrict ourselves to measure the distance between the two intensity maxima of the filaments. This distance varies between 0.3 and 0.37 arcsec (220–270 km). The width of the dark-cored filaments in our observations is thus slightly larger than that reported by Scharmer et al. (2002), which may be a selection effect due to the lower angular resolution of our observations. The length of the dark-cored filaments is significantly larger than their widths. Some of the dark-cored filaments in our images can be identified as independent structures for more than 3 arcsec (~2000 km). We also note that there are filaments that do not exhibit dark cores, as seen, e.g., in Fig. 2c at $y \sim 0.4$ arcsec and in Fig. 2d at $y \sim 1.7$ arcsec. If dark cores were present in these filaments, they would be substantially narrower than 0.2 arcsec and/or have much less pronounced intensity dips.

3.2. Temporal evolution

It is not difficult to find small, dark structures between two bright ones in a filamentary scene like the penumbra. The structures at $(x, y) \sim (21, 20.5)$ and $(18.5, 12)$ in Fig. 1, for instance, do not look much different from our examples presented as dark cores, but in reality they are inter-filament gaps. What makes the dark cores special is the coherency of the motion of the constituent parts when observed over long time periods. Figure 3 displays the temporal evolution of a dark-cored filament during 75 min (see also `AR10425b.mpg` as online material). At the beginning, the core is connected (or identical?) to a dark filament extending over 4.5 arcsec (~3200 km) across the inner penumbra. The two lateral edges end in the same area that shows a slight brightening. This "grain" migrates down and right into the umbra, covering a distance of roughly 725 km

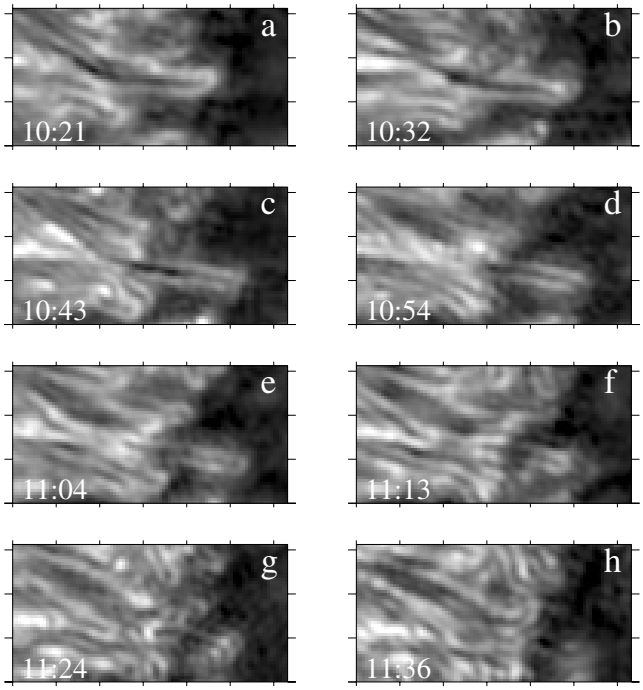

Fig. 3. Temporal evolution of a dark-cored filament between 10:21 **a)** and 11:36 UT **h)**. For better visibility a non-linear intensity scale (γ = 1.6) is used. Tick marks are arcsec.

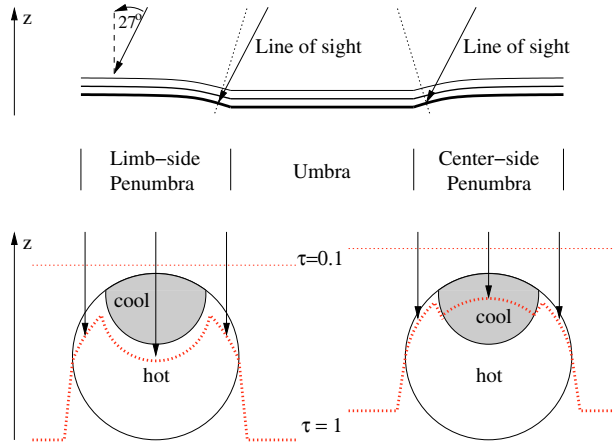

Fig. 4. *Top*: Sketch of isotherms in a sunspot observed at an heliocentric angle of 27 deg. The arrows indicate lines of sight intersecting the center and limb-side penumbra. The dotted lines represent the normal to the isotherms. *Bottom*: Cross section of the same penumbral flux tube observed in the limb-side (*left*) and center-side (*right*) penumbra. The shaded areas in the tube interior represent plasma at lower temperature. The dotted lines mark isolines of optical depth. Depicted are three rays piercing the central and lateral parts of the tube. In the center-side penumbra, $\tau = 1$ is reached in the top part of the tube along the central ray, and in the hotter interior along the lateral rays. This would be observed as two bright streaks separated by a central obscuration.

in 43 min (apparent velocity $\sim$280 m s^{-1}) before it fades to invisibility (frames a–f in Fig. 3). All the time the structure moves as a unit, keeping the two lateral brightenings parallel with a dark separation in between. As in other cases, the intensities of the edges of the dark-cored filament change both in time and along the filament, not necessarily in synchrony. In frame g, only the trailing part of the filament remains visible. The length of the dark-cored filament greatly reduces during the whole process, mainly because it is overlaid by some following structures. This scenario has also been mentioned by Rouppe van der Voort et al. (2004). The filament in Fig. 3 was one of the most durable in our data set, others were as short-lived as 20 min. The long-lived ones were located closer to the umbral border or even extending into the umbral area like the presented example, so it cannot be excluded that their longer lifetime is related to the better visibility due to the higher local contrast.

During their evolution, some of the dark-cored filaments are seen to split into two identical offspring which also possess dark cores. The fragmentation occurs at the position of a bright grain, located either at the inner footpoint or at some distance from it in one of the edges of the parent filament. After fragmentation, the two dark-cored filaments move independently along more or less symmetrically deflected trajectories.

4. Discussion and summary

We have shown that the dark-cored penumbral filaments observed by Scharmer et al. (2002) at very high angular resolution in a sunspot near the disk center can also be found within spots outside the disk center, even at about half the resolution. The consistent detection of these structures over long time spans and in different wavelengths rules out that they are artifacts of seeing or image processing. We confirm the dimensions ($\sim$200–250 km, as measured from the lateral brightenings) and lifetimes (around 1 h) of these structures. In addition we observe a clear asymmetry in the occurrence of dark cores, finding them only in the center-side penumbra.

In the following we speculate that projection effects may cause the observed asymmetry between the center and limb-side penumbra. In the inner penumbra, we expect isotherms to be tilted upwards away from the umbra as in a tilted plane-parallel atmosphere. The tilt may either be due to the Wilson depression or to the presence of hot penumbral flux tubes that heat their surroundings (Fig. 4, top panel). Bellot Rubio et al. (2003) suggest that the flux tubes are inclined upwards by 20 deg in the inner penumbra, and this is the tilt we use for the isotherms represented in Fig. 4. Thus, lines of sight intersecting the center-side penumbra are more inclined relative to the isotherms than those piercing the limb side. Thus, the $\tau = 1$ level is reached in slightly higher layers on the center side.

s Now assume that each bright filament traces a single hot penumbral flux tube embedded in a cool atmosphere and, further, that the top part of the tube is cooler than its interior, as sketched in Fig. 4 (bottom panel). Such a temperature structure is obtained for horizontal flux tubes if one solves for the heat transport in stationary equilibrium for a stratified umbral atmosphere (Ruiz Cobo, private communication). It may also be the result of a hot tube that cools (dynamically) in a stratified atmosphere. Since rays on the center side sample higher geometrical heights, the cool plasma at the top of the tube may become visible in the form of a dark core. On the limb side, the $\tau = 1$ level is reached deeper into the hot tube, making the dark core invisible. This mechanism could also explain the higher

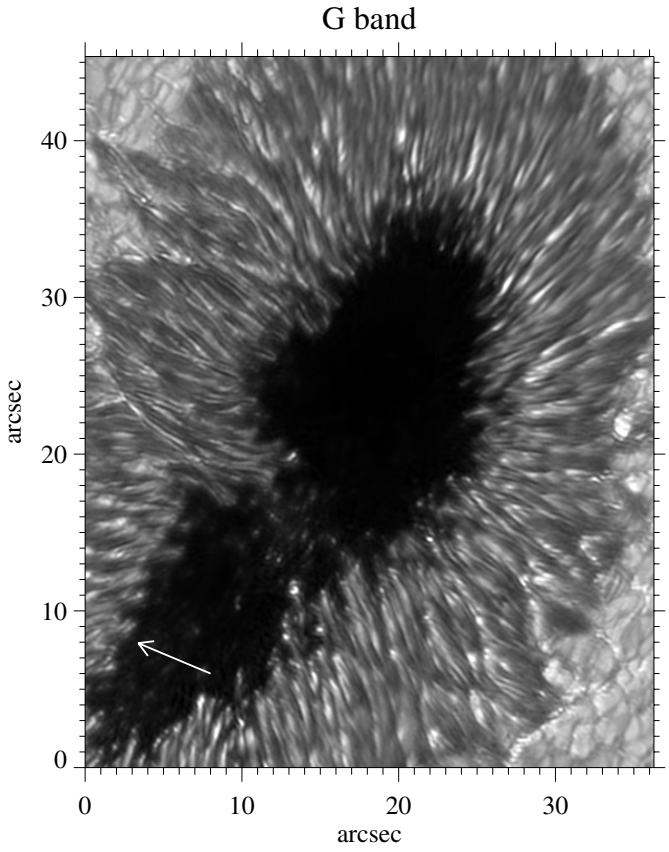

Fig. 5. Subfield of a *G*-band filtergram of NOAA 10008 taken on June 28, 2002. The arrow depicts the direction towards disk center. The heliocentric angle of the spot is 48 deg (μ = 0.67). Consistent with our findings, dark-cored filaments are observed predominantly in the center-side penumbra.

intensity contrast of the dark cores in the *G* band relative to the blue continuum, taking into account that the *G*-band intensities are formed slightly higher up in the atmosphere.

The assumption that isotherms are tilted upwards may also explains the observation that limb-side penumbral grains show larger intensities.

The different morphology of penumbral filaments on the center and limb side described in this paper is also seen in other spots. An example is given in Fig. 5 for a spot at a heliocentric angle of 48 deg. This spot has not been included in this investigation since the time series available is not long enough to trace the evolution of the dark-cored filaments.

Acknowledgements. We thank B. Ruiz Cobo for sharing his calculations with us prior to publication. This information was essential to prepare Fig. 4. W. Schmidt made valuable comments on the manuscript. The DOT project is funded by Utrecht University, the Netherlands Graduate School for Astronomy NOVA and the Netherlands Organization for Scientific Research NWO. P. Sütterlins research is supported by NWO. We acknowledge financial support by the Deutsche Forschungsgemeinschaft under project SCHL 514/2–1.

References

Bellot Rubio, L. R. 2004, Rev. Modern Astron., 17, 21
Bellot Rubio, L. R., Balthasar, H., Collados, M., & Schlichenmaier, R. 2003, A&A, 403, L47
de Boer, C. 1993, Ph.D. Thesis, Universität Göttingen
de Boer, C. R., & Kneer, F. 1992, A&A, 264, L24
Rouppe van der Voort, L. H. M., Löfdahl, M. G., Kiselman, D., & Scharmer, G. B. 2004, A&A, 414, 717
Rutten, R. J., Hammerschlag, R. H., Bettonvil, F. C. M., Sütterlin, P., & de Wijn, A. G. 2004, A&A, 413, 1183
Scharmer, G. B., Gudiksen, B. V., Kiselman, D., Löfdahl, M. G., & Rouppe van der Voort, L. H. M. 2002, Nature, 420, 151
Schlichenmaier, R. 2002, AN, 323, 303
Solanki, S. K. 2003, A&AR, 11, 153
Tritschler, A., Schlichenmaier, R., Bellot Rubio, L. R., & the KAOS Team 2004, A&A, 415, 717
Weigelt, G. P. 1977, Opt. Commun., 21, 55